2020-01-0826 Published 14 Apr 2020

High-Fidelity Simulation of Primary Breakup of a "Spray G" Gasoline Jet with an Adaptive Mesh Refinement and Volume-of-Fluid Method

Yue Ling and Bo Zhang Baylor University

Citation: Ling, Y. and Zhang, B., "High-Fidelity Simulation of Primary Breakup of a "Spray G" Gasoline Jet with an Adaptive Mesh Refinement and Volume-of-Fluid Method," SAE Technical Paper 2020-01-0826, 2020, doi:10.4271/2020-01-0826.

Abstract

Primary breakup of a liquid jet is a process of enormous complexity, involving interfacial dynamics, topology changes, and turbulence. In macro-scale simulations for practical problems, the primary breakup is usually too expensive to be fully resolved and thus is typically represented by phenomenological models. The recent advancement of numerical methods and computer power enables large-scale high-fidelity simulations of primary breakup. The high-level details provided by simulation can be used to verify the assumptions made in existing models and also to develop new models through both physics- or data-based approaches. The present paper will present the state-of-the-art high-fidelity simulation of the primary breakup of a gasoline surrogate jet. The simulation parameters were chosen following the Engine Combustion Network (ECN) ``Spray G" conditions and thus are similar to realistic engine conditions. The surrogate fuel has a low volatility so fuel evaporation does not occur in the atomization process. The present study focuses on the near field where inter-jet interaction is not important and only one of the eight jets in the original injectors is simulated. In the numerical model, the liquid is injected from the inner-hole, through the counterbore, into a chamber with pressurized stagnant gas. An angle between the injection velocity and the inner-hole axis is introduced to mimic the effect of internal flow over the needle into the inner-hole. A parametric study on the inlet angle was performed, and the numerical results are compared to the experimental data (Duke et al., Exp. Therm. Fluid Sci. 88 608-621, 2017) for the jet deflection angle and the temporal variation of penetration length to identify the proper inlet angle to be used in the model. The Basilisk solver was used for the present simulation, in which the gas-liquid interface is captured by the geometric volume-of-fluid method, and an octree mesh is use to discretize the domain to allow local adaptive mesh refinement in regions with interface and small flow scales.

Introduction

A comprehensive understanding of the injection and atomization of gasoline fuels is essential to improving gasoline direct injection (GDI) engines. The breakup of the injected fuel has a direct impact on subsequent turbulent dispersion of the fuel droplets and the mixing of fuel vapor with air, which in turn influence spark ignition and flame propagation [1]. Due to the increasing demand of high fuel efficiency and low pollutant emission, extensive research efforts have been directed toward understanding and predicting atomization process and resulting spray characteristics for gasoline jets in the past decades [2,3,4,5,6, 18].

Primary breakup of a liquid jet involves processes occurring in a wide range of spatial scales. The internal flow inside the injector also has a strong impact on the breakup dynamics of the liquid jet outside the injector, which further complicates the problem [19,24]. Experiment has been the major approach to investigate gasoline injection in the past [2, 3, 4, 5, 6]. However, even with the most advanced optical and X-ray diagnostics, there remain two-phase flow details that are hard to measure in experiments [7,3]. Therefore, numerical simulation is an important alternative to understand the underlying flow physics [9, 10, 11, 12]. Due to the wide range of length scales involved in fuel injection and atomization, a direct numerical simulation that can fully resolve all the scales is generally too expensive. In macro-scale simulations of practical problems, a low-fidelity approach is usually adopted [25, 26, 27]. Different models are then required to represent the unresolved multi-phase flow physics. The unresolved turbulent fluctuations in the gas flow and their influences on the mean flows are modeled by turbulence models such as the k-ε turbulence model [21]. The injected liquid is modeled by discrete parcels (one parcel represents multiple physical droplets) and traced in the Lagrangian framework [28]. In such a case, the drag force and heat transfer models are required to account for the unresolved interaction between the droplets and surrounding gas, so that the motion and temperature evolution of the droplets can be captured [29, 30, 31]. Under certain conditions, the droplet may break due to the aerodynamic force. The Kelvin-Helmholtz/Rayleigh-Taylor (KH-RT) droplet breakup model has been developed to capture the aerodynamic breakup of droplets [8].

The recent rapid development of numerical methods and computer power makes large-scale high-fidelity simulation of

the primary breakup of liquid jets viable [9, 10, 11]. Due to the high computational costs of these high-fidelity simulations, the injection conditions are usually significantly simplified, e.g., the injection velocities are typically an order of magnitude lower than practical engine conditions [32]. Furthermore, the internal flow details inside the injector, which are important to the primary breakup dynamics [19], were usually ignored and simple velocity profiles (such as a uniform velocity profile) were specified at the inlet [9]. Recent attempts have been made to perform high-fidelity simulation for primary breakup of liquid jets produced with practical injector geometry [12, 13, 20, 21, 22]. Nevertheless, whether the mesh resolutions in these previous simulations were sufficient to fully resolve the both the internal flow and the external turbulent sprays remains to be explored.

The goal of the present paper is to demonstrate the state-of-the-art capability of high-fidelity simulations in resolving primary breakup of a liquid jet under engine-relevant operation conditions. We aim at performing a high-fidelity simulation of gasoline jet with operating conditions and injector geometry that better represent realistic engine conditions. The Engine Combustion Network (ECN) ``Spray G" injector is employed and modeled. Even though the present geometry is still significantly simplified, compared to the spray-G injector, the boundary conditions at the inlet are carefully calibrated based on the X-ray experiment by Duke et al. [3], so that the model will capture the dominant effect of the internal flow on the liquid jet breakup. To allow a direct comparison between the numerical and experimental results, a low-volatility gasoline surrogate is used as in the experiment. As a result, fuel evaporation is ignored. The adaptive multiphase flow solver, Basilisk, is used for the simulation. The details of the numerical methods used in the solver are given as follows.

Simulation Methods

The one-fluid approach is employed to resolve the gas-liquid two-phase flow in the present problem. The phases corresponding to the liquid fuel and the free stream air are treated as one fluid with material properties that change abruptly across the interface. The incompressible, variable-density Navier-Stokes equations with surface tension are written as

$$\rho\left(\partial_t \mathbf{u} + \mathbf{u}\cdot\nabla\mathbf{u}\right) = -\nabla p + \nabla\cdot\left(2\mu\mathbf{D}\right) + \sigma\kappa\delta_s\mathbf{n}, \quad (1)$$

$$\nabla\cdot\boldsymbol{u} = 0 \quad (2)$$

where ρ, μ, $\boldsymbol{u}$, and p represent density, viscosity, velocity, and pressure, respectively. The deformation tensor is denoted by $\boldsymbol{D}$ and has components $D_{ij} = (\delta_i u_j + \delta_j u_i)/2$. The third term on the right-hand side of Eq. (1) is a singular term representing the surface tension force, containing a Dirac distribution function δ_s localized on the interface. The variable σ represents the surface tension coefficient and the variables κ and n represent the local curvature and unit normal of the interface, respectively.

The tracer function C (also known as the volume fraction function) is introduced to distinguish the different phases: C=1 and 0 in the computational cells with only liquid and gas, while C is fractional in the cells with the gas-liquid interface. The time evolution of C follows the advection equation

$$\partial_t C + \boldsymbol{u}\cdot\nabla C = 0 \quad (3)$$

which is solved by a geometric volume-of-fluid method [11].

Numerical Methods

The Navier-Stokes equations (Eqs. (1) and (2)) are solved by the open-source solver, *Basilisk*. A finite volume approach based on a projection method is used. The Crank-Nicholson discretization of the viscous terms and the Bell-Colella-Glaz second-order unsplit upwind scheme for the velocity advection term are both second-order accurate [17, 23]. A staggered-in-time discretization of the volume-fraction/density and pressure leads to a formally second-order accurate time discretization. The interfaces between the different fluids are tracked and followed using a Volume-of-Fluid (VOF) method [11]. A momentum-conserving VOF (MCVOF) method is used to advect the volume fraction and momentum in a consistent manner, so that both mass and momentum conservations are achieved [14, 15]. An octree spatial discretization is used, which gives a very important flexibility allowing dynamic grid refinement into user-defined regions [12]. Finally, the height-function (HF) method is utilized to calculate the local interface curvature, and a balanced-force surface tension discretization is used [16, 17]. The parallelization of the solver is done through a tree decomposition approach to guarantee a high parallel performance even if a large number of refinement levels are used.

Simulation Setup

The original Spray G injector has eight holes, so eight liquid jets will be generated. As shown in experimental images, the jets are spatially separated and do not interact with each other in the near field [3, 6]. To focus computational resources on capturing the liquid jet breakup in the near field, only one of the original eight jets is considered here. Furthermore, the numerical model will only consider the inner-hole and counterbore of the injector, with the portion upstream of the inner-hole (including the needle) ignored, see Fig. 1(a). To model the effect of the liquid flow over the needle into the inner-hole, the liquid velocity at the inlet of the inner-hole is considered to be not perfectly aligned with the inner-hole axis. The angle between the inlet velocity and the inner-hole axis, α, is simply referred to as the "injection angle" hereafter for convenience. The component of the inlet velocity, U_j, that is normal to the inlet plane is determined by the injection mass flow rate, which is kept as constant [3]. The tangential components of the inlet velocity are represented by V_j and W_j, which are along y and z axes, respectively. The magnitude of the tangential inlet velocity is $V_t = \sqrt{V_j^2 + W_j^2}$, which varies with the injection angle, α. The ratio between V_t and U_j is equal to the tangent of the inlet angle, namely, $\eta = |V_t/U_j| = \tan\alpha$. The non-zero injection angle results in a deflection and breakup of the liquid jet (details will be shown later), and thus has been included to accurately capture the bulk jet and breakup dynamics.

FIGURE 1 Simulation setup for the gasoline surrogate jet: (a) the whole computational domain (grey color indicates the solid nozzle); (b) a closeup of the inner hole, counterbore, and the liquid jet near the nozzle exit; (c) a schematic showing the angle between the injection velocity and the inner hole axis, α, and the angle between the jet axis and the inner hole axis, β; (d) the definition of a cylindrical coordinate on the y-z plane.

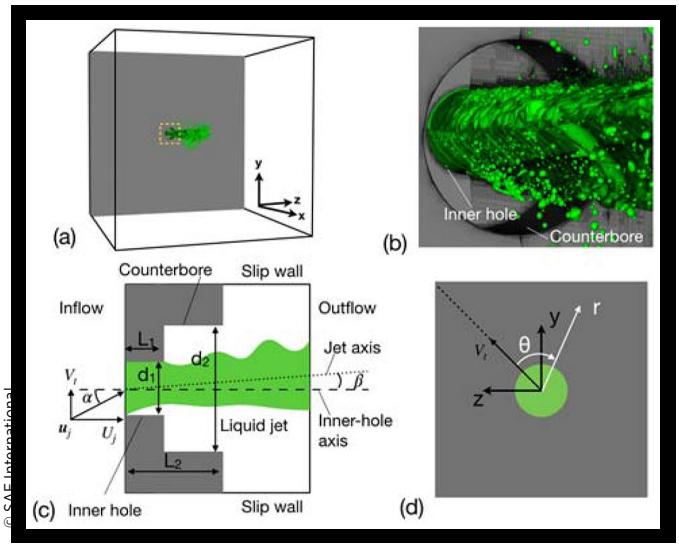

Two different approaches have been used to specify velocity boundary conditions at the inlet, mainly for the tangential inlet velocity components V_j and W_j: 1) V_j=V_t, and W_j=0, so the tangential velocity is aligned with the y axis, and 2) $V_j = W_j = V_t / \sqrt{2}$, so the tangential velocity is 45 degrees with respect to the y axis, as shown in Fig. 1(d). The results for these two setups are shown in Figs. 2(a) and (b). It can be observed that the second approach yields more accurate results. The numerical error introduced a numerical artificial effect along the Cartesian mesh in setup 1), see the "fin" on the top of the liquid in Fig. 2(a). This artifact was eliminated in setup 2). Therefore, the results in the rest of the paper correspond to the second setup, see Fig. 2(b).

The transient injection velocity due to needle motion is also ignored and the rate of injection is constant. The computational domain is shown in Fig 1 (a), where the grey color indicates the solid nozzle. A closeup of the inlet is given in in Fig. 1(b), from which the inner-hole, the counterbore, and the liquid jet morphology in the near field can be identified. The dimensions of the inner hole and counterbore are listed in Table 1. For convenience of discussion on the azimuthal and radial variation of fluid properties, a cylindrical coordinate is also defined on the y-z plane, as indicated in Fig. 1(d). The azimuthal angle, θ, is defined with respect to the tangential inlet velocity.

The liquid velocity at the inlet is considered as uniform. The boundary layer near the nozzle wall will develop only after the liquid enters the nozzle innerhole. The effect of the non-uniform velocity distribution at the inlet is considered to be secondary and is ignored in the present model. The good agreement between the simulation and experimental results for penetration length and deflection angle seems to support this simplification.

FIGURE 2 Morphology of the atomizing jet near the nozzle exit from the side view for four different simulation setups at 19.4 μs. The conventional VOF method is used for (a) and (b), while the momentum-conserving VOF method is used for (c) and (d). The tangential velocity at the inlet is specified as V_j=V_t, and W_j=0 for (a) and $V_j = W_j = V_t / \sqrt{2}$ for (b). The maximum refinement level is 11 for (a)-(c) and is 12 for (d).

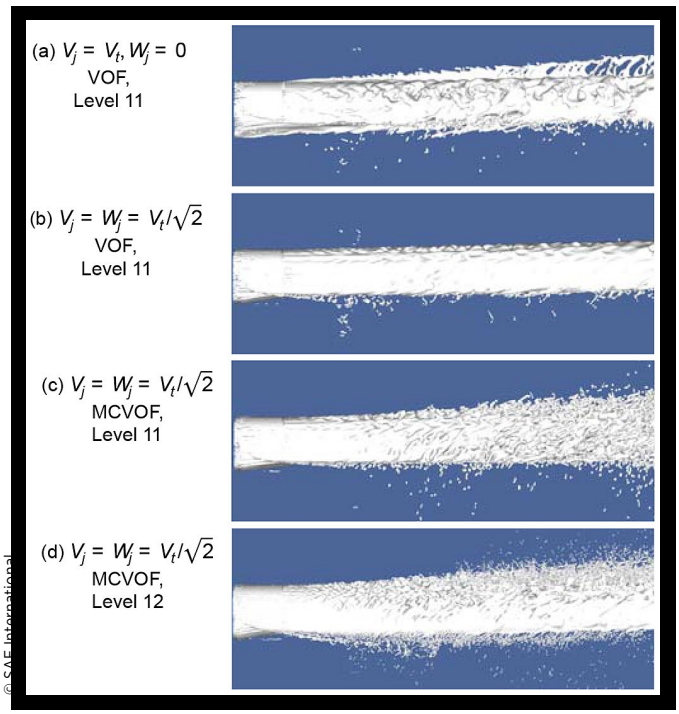

TABLE 1 Parameters of the nozzle geometry and injection velocities.

d_1	d_2	L_1	L_2	U_j	V_t
173 (μm)	388 (μm)	152 (μm)	395 (μm)	89 (m/s)	0 - 35.6 (m/s)

TABLE 2 Liquid and gas properties used in the present study, which are consistent with the experiment [3].

ρ_l	ρ_g	μ_l	μ_g	σ
838 (kg/m^3)	3.6 (kg/m^3)	9.64e-4 (Pa s)	1.77e-5 (Pa s)	0.0278 (N/m)

The fluids properties and the injection conditions are chosen to be similar to the X-ray experiments by Duke et al. [3], and are listed in Table 2. The liquid in the experiment was a low-volatility gasoline surrogate (Viscor 16br, Rock Valley Oil & Chemical Company) with a cerium contrast agent (Rhodia DPX9) [3]. Due to the low vapor pressure in the chamber and the use of low-volatility fuel surrogate, evaporation is ignored in the present simulation. The gas in the chamber is nitrogen, with a pressure and temperature of 3.15 bar and 298 K, respectively. The density and viscosity of the gas are 3.6 kg/m^3 and 1.77×10^{-5} Pa s, respectively. The density of ambient gas is similar to the original Spray G condition.

The minimum cell size in the simulation is controlled by the maximum refinement level. Two different levels have been used. The levels 11 and 12 correspond to the minimum cell size of 2.7 and 1.35 μm, respectively. As will be shown later, the level 12 mesh is sufficiently fine to capture the small-scale interfacial waves on the jet surfaces. The minimum cell size of 1.35μm may be not fine enough to resolve all the droplets generated in the atomization process, but is expected to capture majority of droplets formed.

A direct numerical simulation (DNS) approach is used in the present study. Therefore, there is no turbulence model involved. The Kolmogorov scale is estimated as $\eta \approx (\upsilon_g^3 / (U_j^3 / D_j))^{\frac{1}{4}} = 0.41\,\mu m$, the minimum cell size for the finest mesh used is Δ=1.35 μm. According to the general DNS resolution criterion $\Delta/\eta \lesssim 2.1$ [33], the current mesh resolution is not far from fully resolving the smallest turbulent eddies.

Since an adaptive mesh is used here, the number of cells increases over time, when more and more liquids are injected into the domain. The maximum number of octree cells for level 12 is about 200 million. The total computational time for all cases presented here is about 400,000 CPU core-hours. The simulations for levels 11 and 12 were run with 144 and 1440 CPU cores (Intel Xeon Platinum 8160) for 3 and 6 days, respectively.

Results

Effects of Numerical Methods & Mesh Resolution

The results obtained with two different VOF methods, namely the conventional VOF and the MCVOF methods, are shown in Figs. 2(b) and (c). It can be observed that the macro-scale features are similar but more small-scale liquid structures, like thin sheets and ligaments, are captured with MCVOF. Due to the large liquid-to-gas density ratio, the numerical error for not conserving momentum will introduce fake breakup of liquid structures [10]. The results for using two different mesh resolutions, namely levels 11 and 12, are shown in Figs. 2(c) and (d). With the finer mesh, small-scale features, such as the formation of small droplets, are better resolved.

Effects of Injection Angle

When the head of the jet interacts with the stationary gas, liquids are pushed radially outward and form a liquid sheet rolling up. As the liquid jet core advects downstream with a faster speed, the rolled-up liquid sheet flaps backward forming the mushroom head. This mushroom-like shape of the jet head (see Fig. 3(a)) has also been observed in former studies [9]. Simultaneously, the surrounding gas is entrained into the bottom region of the inner hole owing to the reversed flow of the gas caused by the lower local pressure, which is due to the effect of injection angle shifting the jet core towards the upper edge of the inner hole, see Fig. 3(a). In addition, the non-zero injection angle changes the transverse distribution of velocity

FIGURE 3 Deformation and breakup of the head of the liquid jet from side (a-d) and front (e-h) views. The liquid surface is colored by the streamwise velocity.

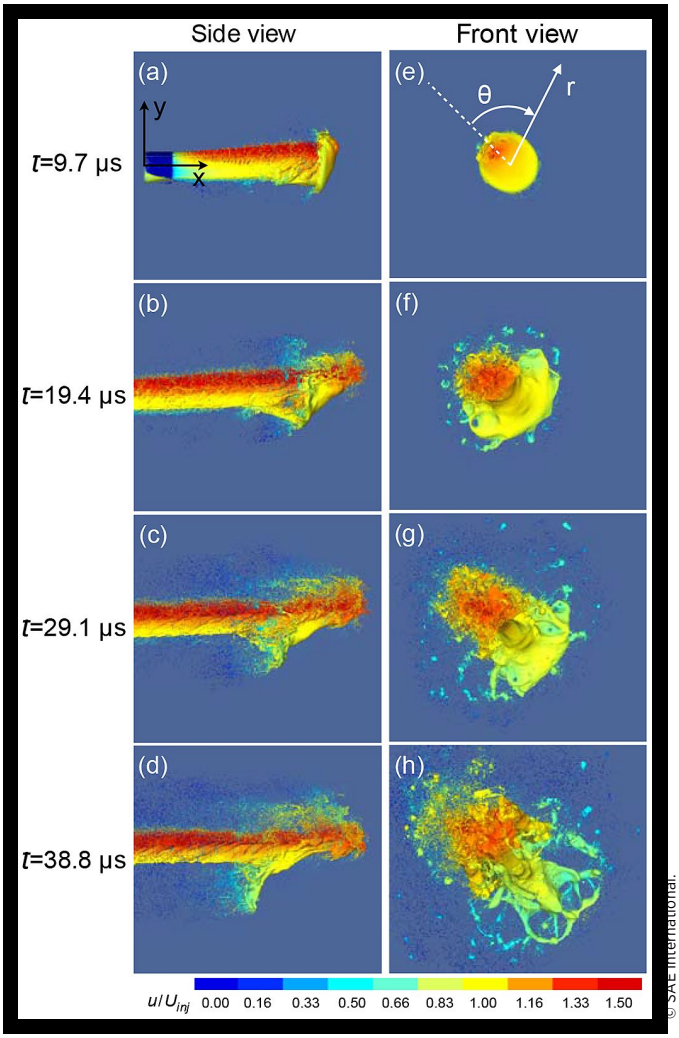

within the jet: at the same streamwise location the top of the jet moves faster than the side and the bottom (see Fig. 3). As a result, the head is stretched along the streamwise direction and the streamwise width of the jet head increases over time, which will thus result in a smearing profile of the transverse integrated mass (TIM) near the jet head (see Fig. 4), where TIM is defined as

$$TIM(x,t) = \iint \rho(x,y,z,t)\,dy\,dz$$

Since the penetration length of the jet is typically defined based on TIM, the value of penetration length is sensitive to the threshold of TIM used in definition.

To allow a direct comparison of penetration length evolution with the experiment, the same TIM threshold (20%) is used for the simulation results. The temporal evolutions of the jet penetration length for different injection angle, characterized by η=tanα, are shown in Fig. 5(a). Consistent with the experimental data, the simulation results for the penetration length increase almost linearly with time during the time range considered. The penetration velocity (the slopes of the lines) generally increases with η. The simulation result for η

FIGURE 4 Temporal evolution of transverse integrated mass (TIM).

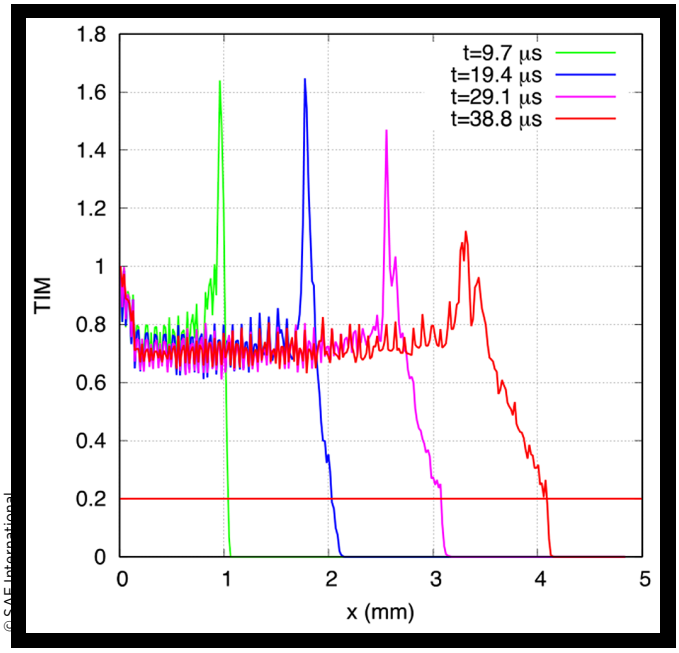

= 0.2 is shown to agree well with the experiment. The increase of penetration with injection angle is due to deformation of the liquid jet. When a non-zero injection angle is present, the liquid jet detaches from the lower edge of the inner hole, resulting in a decrease of the cross-section area and large velocity in the liquid.

Another important effect of the injection angle is on the deflection of the bulk liquid jet. The deflection angles for different η are shown in Fig. 5(b). The deflection angle is defined as the angle between the liquid jet central axis (the ensemble of centroid of liquid mass in different streamwise cross sections) and the inner hole axis, consistent with the experiment [3]. The results shown in Fig. 5(b) are measured at about x/D=11. Data at the measurement location is not available until the arrival of the jet head. The initial large-amplitude fluctuations are due to the passage of the jet head. After that, the evolution of the deflection angle reaches a quasi-steady state with some fluctuations. These fluctuations are in turn due to the interfacial waves on the jet surface.

Breakup of the Jet Head

As time elapses, the jet head is stretched significantly and the top of the mushroom head first broke due to the higher streamwise velocity near the top of the jet (see Fig. 3). Holes were observed in the liquid sheet. The holes expand quickly due to the retraction of the Taylor-Culick rims. Eventually, these holes merge and disintegrate the liquid sheet into small ligaments and droplets. The breakup gradually extends toward the lower part of the jet head. Some droplets generated from the breakup of the upper part of the mushroom head were observed to impinge on the liquid sheets and further enhance the breakup of the jet head. At about 38.8 μs, the whole jet head is almost fully broken up.

FIGURE 5 Temporal evolution of (a) the liquid jet penetration and (b) the plume angle deviation from the drill angle for different inlet angle (η=tanα). The simulation results are compared with the experimental data [3].

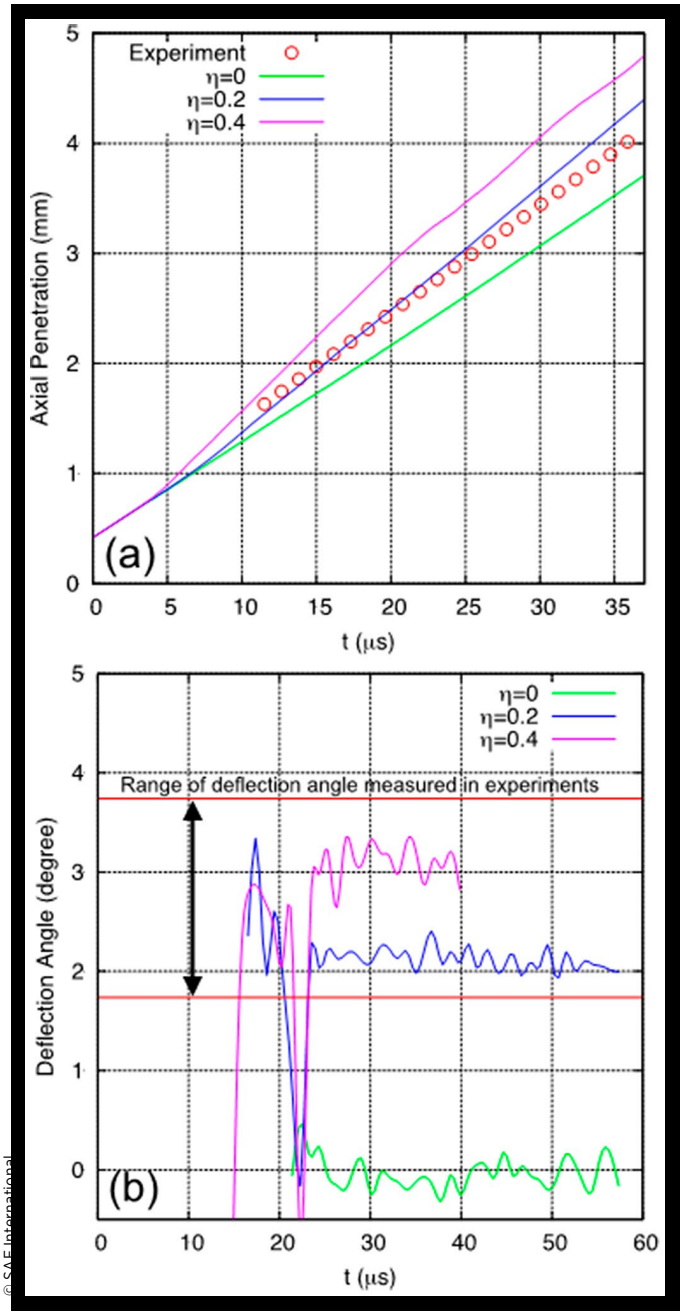

In terms of the number of droplets generated, the disintegration of the jet head seems to produce significantly more droplets than the shear-induced breakup on the surface of the jet core. Therefore, the breakup dynamics of the jet head is important to the ultimate drop size distribution obtained downstream.

Droplet Size Distribution

The droplets size distributions at t = 28.1 μs are shown in Fig. 6. Here, the drop size is calculated based on droplet

FIGURE 6 Droplet size distribution for (a) and probability distribution function (PDF) profiles of droplet number (b) in terms of volume-based diameter for distinct azimuthal angle ranges at 28.1 μs with the exponential and lognormal distribution functions fitting the PDF curve of 0< θ < 30 degrees. The vertical dashed lines in (a,b) indicate twice of the smallest mesh size.

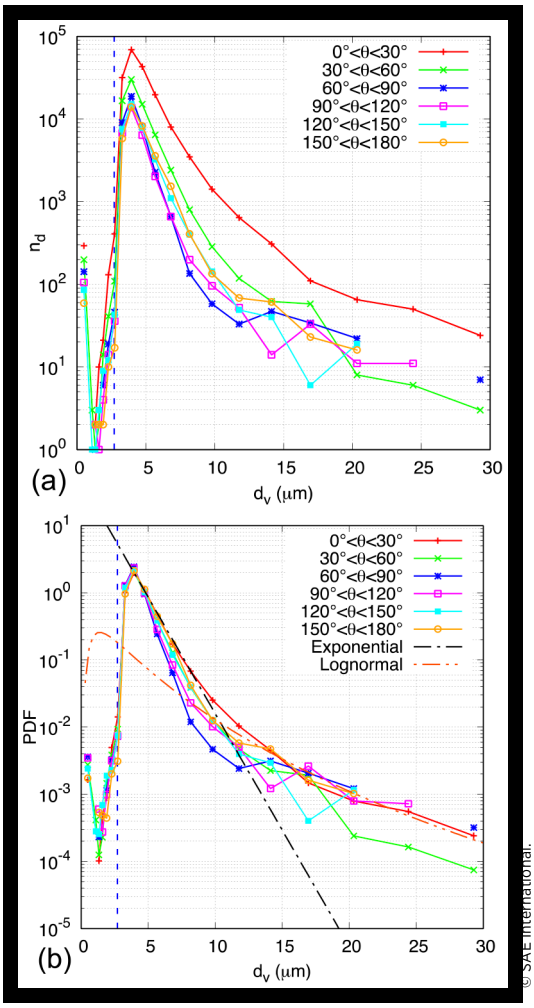

volume. Here, n_d represents the number of droplets of size within the bin width, and is averaged over a short sampling time of about 1.9 μs, namely from 27.2 to 29.1 μs. Though the present atomizing flow is highly unsteady, the results indicate that the profile of the PDF at later time (t>15 μs) is not sensitive to the sampling time duration. Since the PDF is calculated based on all the droplets in the domain, namely accounting for all the droplets generated in the history, the droplets generated within the short sampling time duration takes only a small portion of the overall droplets and thus their effect on the overall PDF profile is small. The purpose of averaging the PDF over a short time duration, instead of using a single snapshot, is simply to increase the number of droplets and thus to reduce the fluctuations in the PDF profiles for large droplets, see for example d_v>12 μm in Fig. 6(a). Furthermore, a non-uniform bin width is adopted also to reduce the fluctuations for larger droplets.

FIGURE 7 Droplet number-based and volume-based PDF for all droplets in the domain at 38.8 μs. The vertical dashed line indicates twice of the smallest mesh size.

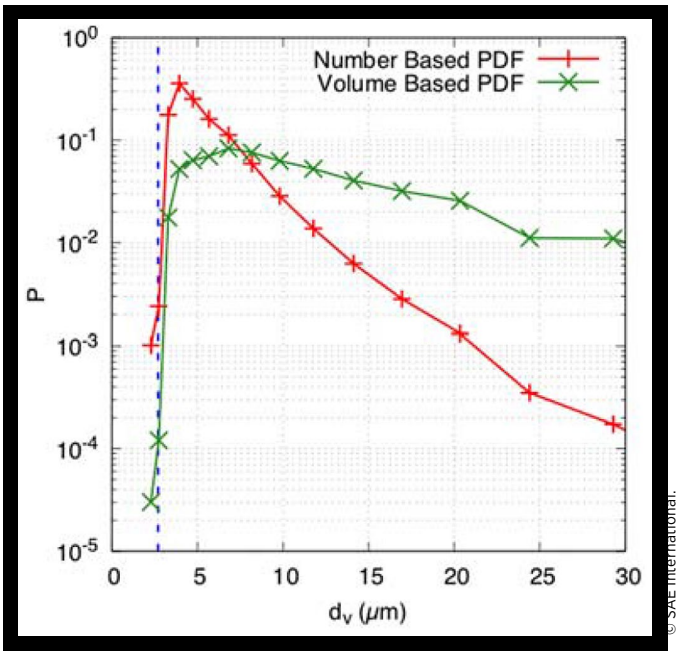

The focus here is to show the azimuthal variation of the droplets number and size distribution which is induced by the asymmetric breakup of the liquid jet, in particular for the jet head. As can be seen in Fig. 6 (a), the number of droplets for small θ (namely at the top of the jet) is significantly larger. This is consistent with the observation that the breakup of the jet head is more intense for small θ than larger θ. When the droplets number is plotted as the probability distribution functions (PDF), it is observed that the PDF profiles for different angles are indeed quite similar, see Fig. 6 (b). There exist small discrepancies at the tail of the PDF profiles for different θ.

The exponential and lognormal distribution functions have been employed to fit the PDF curves. Yet none of them seem to recover the whole PDF profiles. The exponential function captures well the early decay of the tail, but not for the range of larger droplets. The log-normal function fits well the range of larger droplets yet it fails to capture the peak and the range for smaller droplets.

Finally, the volume-based PDF for all the droplets in the domain at 38.8 μs are compared with the number-based PDF in Fig. 7. The vertical line in the figure indicates twice of the smallest mesh size (2.7 μm here for mesh refinement level 12). The formation of droplets smaller this threshold may not be sufficiently resolved, and thus the data are less trustworthy. Nevertheless, it is observed that peaks of the droplet number- and volume-based PDF are about 4 and 8 μm, which are about 3 and 6 time of the minimum cell size, respectively. Therefore, although present mesh resolution will not fully capture the sub-microns droplets, the majority of the droplets formed are captured in terms of both droplet number and volume (or mass).

Summary

The primary breakup of a gasoline surrogate jet has been investigated in this study through high-fidelity simulation. The numerical model is developed based on the spray G injector geometry and operation conditions. In order to focus computational resources on the interfacial dynamics and liquid breakups, the injector geometry is simplified and only one jet is considered. The dominant effect of the internal flow in the injector on atomization is modelled by the non-zero inlet angle between the inflow velocity and the nozzle inner-hole axis. The simulation results for different inlet angles were compared with the X-ray experimental results using the full spray G injector to identify the proper inlet angle to be used in the numerical model. It is shown that the numerical results of the jet penetration length and the deflection angle for $\eta = 0.2$ match well with the experimental data and thus the model for $\eta = 0.2$ is expected to be a good approximation for the near-field dynamics of the atomizing jet. Details of the primary breakup, in particular, near the head of the jet were well resolved, and strong asymmetric breakup dynamics was observed. The asymmetry in the breakup process results in asymmetric droplet statistics. The azimuthal variation of droplets statistics is important to the overall spatial distribution of liquid volume fraction. An accurate primary breakup model has to take this into account, yet that is out of the scope of the present paper and will be relegated to the future work.

References

1. Lefebvre, A.H. and McDonell, V.G., *Atomization and Sprays* (CRC Press, 2017).
2. Mitroglou, N., Nouri, J.M., Gavaises, M., and Arcoumanis, C., "Spray Characteristics of a Multi-Hole Injector for Direct-Injection Gasoline Engines," *Int. J. Engine Res.* 7(3):255-270, 2006.
3. Wang, Z., Swantek, A., Scarcelli, R., Duke, D. et al., "LES of Diesel and Gasoline Sprays with Validation Against x-ray Radiography Data," *SAE Int. J. Fuels Lubr.* 8:147-159, 2015, https://doi.org/10.4271/2015-01-0931.
4. Duke, D.J., Kastengren, A.L., Matusik, K.E., Swantek, A.B. et al., "Internal and Near Nozzle Measurements of Engine Combustion Network "Spray G" Gasoline Direct Injectors," *Exp. Therm Fluid Sci.* 88:608-621, 2017.
5. Khan, M.M., Helie, J., Gorokhovski, M., and Sheikh, N.A., "Air Entrainment in High Pressure Multihole Gasoline Direct Injection Sprays," *J. Appl. Fluid Mech.* 10:1223-1234, 2017.
6. Sphicas, P., Pickett, L.M., Skeen, S.A., and Frank, J.H., "Inter-plume Aerodynamics for Gasoline Spray Collapse," *Int. J. Engine Res.* 19(10):1048-1067, 2018.
7. Heindel, T., "X-Ray Imaging Techniques to Quantify Spray Characteristics in the Near Field," *Atomization Spray* 28:1029-1059, 2018.
8. Beale, J.C. and Reitz, R.D., "Modeling Spray Atomization with the Kelvin-Helmholtz/Rayleigh-Taylor Hybrid Model," *Atomization Spray* 9:623-650, 1999.
9. Shinjo, J. and Umemura, A., "Simulation of Liquid Jet Primary Breakup: Dynamics of Ligament and Droplet Formation," *Int. J. Multiphase Flow* 36:513-532, 2010.
10. Ling, Y., Fuster, D., Zaleski, S., and Tryggvason, G., "Spray Formation in a Quasiplanar Gas-Liquid Mixing Layer at Moderate Density Ratios: A Numerical Closeup," *Phys. Rev. Fluids* 2:014005, 2017.
11. Ling, Y., Fuster, D., Tryggvasson, G., and Zaleski, S., "A Two-Phase Mixing Layer between Parallel Gas and Liquid Streams: Multiphase Turbulence Statistics and Influence of Interfacial Instability," *J. Fluid Mech.* 859:268-307, 2019.
12. Befrui, B., Aye, A., Bossi, A., Markle, L.E., and Varble, D.L., "Ecn gdi spray g: Coupled les jet primary breakup-lagrangian spray simulation and comparison with data," in *ILASS Americas 28th Annual Conference*, 2016.
13. Mohan, B., Jaasim, M., Perez, F.H., Sim, J., Roberts, W., and Im, H., "Internal and Near Nozzle Flow Simulations of Gasoline Multi-Hole Injector (ecn spray g) with Transient Needle Motion," in *Proceedings of the 10th International Symposium on Cavitation*, 2018.
14. Vaudor, G., Menard, T., Aniszewski, W., Doring, M., and Berlemont, A., "A Consistent Mass and Momentum Flux Computation Method for Two Phase Flows. Application to Atomization Process," *Comput. Fluids* 152:204-216, 2017.
15. Fuster, D. and Popinet, S., "An all-Mach Method for the Simulation of Bubble Dynamics Problems in the Presence of Surface Tension," *J. Comput. Phys* 374:752-768, 2018.
16. Francois, M.M., Cummins, S.J., Dendy, E.D., Kothe, D.B. et al., "A Balanced-Force Algorithm for Continuous and Sharp Interfacial Surface Tension Models within a Volume Tracking Framework," *J. Comput. Phys.* 213:141-173, 2006.
17. Popinet, S., "An Accurate Adaptive Solver for Surface-Tension-Driven Interfacial Flows," *J. Comput. Phys.* 228(16):5838-5866, 2009.
18. Payri, R., Salvador, F.J., Marti-Aldaravi, P., and Vaquerizo, D., "ECN Spray G External Spray Visualization and Spray Collapse Description through Penetration and Morphology Analysis," *Appl. Therm. Eng.* 112:304-316, 2017.
19. Payri, R., Gimeno, J., Marti-Aldaravi, P., and Vaquerizo, D., "Internal Flow Characterization on an ECN GDi Injector," *Atomization Spray* 26:889-919, 2016.
20. Agarwal, A. and Trujillo, M.F., "The Effect of Nozzle Internal Flow on Spray Atomization," *Int. J. Engine Res.* 21:55-72, 2020.
21. Sparacino, S., Berni, F., d'Adamo, A., Krastev, V.K. et al., "Impact of the Primary Break-Up Strategy on the Morphology of gdi Sprays in 3d-cfd Simulations of Multi-Hole Injectors," *Energies* 12:2890, 2019.
22. Yue, Z., Battistoni, M., and Som, S., "Spray Characterization for Engine Combustion Network Spray g Injector Using High-Fidelity Simulation with Detailed Injector Geometry," *Int. J. Engine Res.* 21:226-238, 2020.

23. Bell, J.B., Colella, P., and Glaz, H.M., "A Second-Order Projection Method for the Incompressible Navier-Stokes Equations," *J. Comput. Phys.* 85:257-283, 1989.
24. Agarwal, A. and Trujillo, M.F., "The Effect of Nozzle Internal Flow on Spray Atomization," *Int. J. Engine Res.* 21:55-72, 2020.
25. Aguerre, H.J. and Nigro, N.M., "Implementation and Validation of a Lagrangian Spray Model Using Experimental Data of the ecn Spray g Injector," *Comput. Fluids* 190:30-48, 2019.
26. Di-Ilio, G., Krastev, V.K., and Falcucci, G., "Evaluation of a Scale-Resolving Methodology for the Multidimensional Simulation of gdi Sprays," *Energies* 12:2699, 2019.
27. Navarro-Martinez, S., Tretola, G., Yosri, M.R., Gordon, R.L., and Vogiatzaki, K., "An Investigation on the Impact of Small-Scale Models in Gasoline Direct Injection Sprays (ecn spray g)," *Int. J. Engine Res.* 21:217-225, 2020.
28. Dukowicz, J.K., "A Particle-Fluid Numerical Model for Liquid Sprays," *J. Comput. Phys.* 35:229-253, 1980.
29. Maxey, M.R. and Riley, J.J., "Equation of Motion for a Small Rigid Sphere in a Nonuniform Flow," *Phys. Fluids* 26:883-889, 1983.
30. Michaelides, E.E. and Feng, Z., "Heat Transfer from a Rigid Sphere in a Nonuniform Flow and Temperature Field," *Int. J. Heat Mass Transfer* 37:2069-2076, 1994.
31. Ling, Y., Balachandar, S., and Parmar, M., "Inter-Phase Heat Transfer and Energy Coupling in Turbulent Dispersed Multiphase Flows," *Phys. Fluids* 28:033304, 2016.
32. Desjardins, O. and Pitsch, H., "Detailed Numerical Investigation of Turbulent Atomization of Liquid Jets," *Atomization Spray* 20:311-336, 2010.
33. Pope, S.B., *Turbulent Flows* (Cambridge Univ Press, 2000).

Contact Information

Corresponding author: **Yue Ling**, Department of Mechanical Engineering, Baylor University, Waco, TX 76798. stanley_ling@baylor.edu.

Acknowledgments

The authors acknowledge the support of National Science Foundation (NSF #1853193). The simulations presented in this paper were performed on Stampede2 at the Texas Advanced Computing Center cluster (TACC) and also on the Baylor cluster Kodiak.

ISSN 0148-7191